Optimal Retro Reflector Acceptance Angles for Application to Building Skins as a Heat Island Countermeasure Based on Climate Data for Japanese Cities

P. Rajagopalan, V. Soebarto and H. Akbari (Eds.), *6th International Conference on Countermeasures to Urban Heat Islands (IC2UHI)*, pp. 173-182. ©2023, RMIT University, Melbourne, Australia.

Optimal Retro Reflector Acceptance Angles for Application to Building Skins as a Heat Island Countermeasure Based on Climate Data for Japanese Cities

Craig Farnham [1], *Jihui Yuan*[2], *Kazuo Emura*[3]
[1,2,3]*Osaka Metropolitan University, Osaka, Japan*

ABSTRACT

Retro reflective materials (RRM) applied to building skins may be more effective in reducing the net thermal load of sunlight on cities than diffusive highly-reflective materials, which reduce the solar load on individual buildings, but scatter some of that load to surrounding buildings and pavements, contributing to the heat island effect. Selection of appropriate RRM depends in part on the expected angle of incident light. This research calculates total intensity of direct insolation (DI) and its incident angle on building outer walls in the four compass directions over a typical year and extreme year using direct insolation measurement data for 6 major Japanese cites from the span 2010-2018 in the METPV-20 database. The total DI in 10 degree spans of incident angle are compiled for those years and their warm periods (May-October). Results show that south-facing walls are the most important in terms of DI in all locations, but in May-Oct the east and west walls are each nearly equal or more than the south wall. Incident angles of 30°-70° are most important for south walls, but in May-Oct it is largely 60°-80° in most cities. Incident angles for east and west walls are more uniformly distributed over 20°-70°. This information can assist in optimizing the design and application of RRM as a heat island countermeasure. For example, RRM for south walls should be designed for large incident angles, while east/west walls should handle a wider range.

Keywords: Retroreflector, direct insolation, typical year, angle

Introduction

The Urban Heat Island (UHI) presents a challenge to the urbanizing world. One cause is that buildings absorb sunlight, acting as heat sinks. Temperatures in the urban environment increase, yielding increased risk of adverse health effects and increased energy consumption for cooling. Much research is devoted to strategies to mitigate the UHI focusing on this problem of reducing sunlight absorption by buildings such as; cool roofs (Levinson and Akbari 2010), green roofs (Santamoris 2014), shading (Inoue 2007), green building strategies (He 2019), and building coatings (Gobakis *et al*. 2016). Many of these concepts include the use of highly reflective materials applied to building skins (outer walls and roofs), such as white paint.

Highly-reflective building skins can reduce the solar thermal load on buildings by reducing absorption of that heat energy. However, part of this thermal load is reflected to the surroundings. Thus, while the subject building thermal load may be reduced, much of that heat is redirected to the nearby buildings and ground, still contributing to the heat island effect.

[1] Corresponding Author: [farnham@omu.ac.jp], ORCID: 0000-0002-8822-891X
[2] [yuan@omu.ac.jp], ORCID: 0000-0002-1608-9973
[3] [emuraocu@gmail.com], ORCID:

Retro reflective materials (RRM) direct a portion of incident light back along the same path. If used to reflect sunlight from building skins, this reflection back into the sky would remove some of the solar thermal load both from the building to which it is applied and the surroundings (Rossi *et al*. 2014; Yuan *et al.* 2015; Castellani *et al*. 2017; Ichinose, Inoue, and Nagahama 2017) as illustrated in Figure 1. This can yield a net reduction in thermal load for both the RRM-skin building and the area as a whole. Thus, RRM applied to building skins may be more effective in reducing the net thermal load of sunlight on cities than diffusive highly-reflective materials.

Selection of appropriate RRM depends in part on the expected angle of incident light, also termed the "entrance angle" or "acceptance angle", where a light source normal to a surface with applied RRM has an incident angle of 0. The retro-reflectance efficiency depends on the incident angle of light and the structure of the RRM.

Common RRM are comprised of two major types, prisms/cube-corners or glass spheres/lenses (Arrechi *et al*. 2007). Cube-corner RRM typically have a higher retro reflectance efficiency than sphere RRM at small incident angles under 45˚, while glass sphere RRM can have wider acceptance angles but lower overall efficiency as was measured by Yuan *et al*. (2016). An example of light ray tracing interaction with each type, using a ray optics simulation program developed by Tu (2022) is shown in Figure 2. Thus, both types may commonly be used in traffic signs, where the incident angle of vehicle headlights is usually small. Road surface markings often include glass beads in the white or yellow substrate as the incident angle is large. The ASTM standard (ASTM 2018) for road marking RRM evaluation assumes an entrance angle of 86˚.

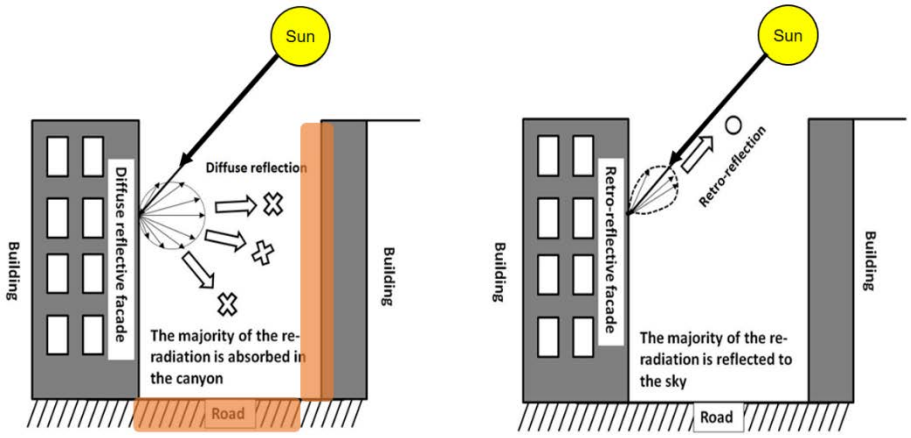

Figure 1. (L) Standard highly-reflective building skins transfer much of the insolation heat load to the surroundings. (R) RRM building skins can reflect it out of the urban space.

Research goal

The goal of this study is to quantify which sunlight incident angles carry the most direct insolation (DI) onto walls, such that a suitable RRM can be selected or designed for the purpose of reflecting sunlight out of the urban space. Here, as a first step, an evaluation of major cities in Japan is done. Continuing to major cities worldwide can yield an atlas of optimal acceptance angles for RRM building skin application as an urban heat island (UHI) countermeasure, analogous to current maps of optimal tilt angles for solar panels (Saint-Drenan et al, 2018) such that material manufacturers can devote resources to creating a UHI-RRM that is optimal for a chosen region or country.

If RRM are applied to building outer walls facing the four compass directions, it could be expected that east and west walls would often be exposed to insolation with small incident

angles, such as near sunrise and sunset. In the northern hemisphere, south-facing walls may be expected to have insolation with large incident angles such as in summer near midday as the sun is high in the sky. However, to select or design new RRM for building skin application as a heat-island countermeasure, this must be quantified in terms of acceptance angle and insolation.

In this study, direct insolation and its distribution over incident angles onto wall surfaces is calculated. The clear-sky ideal insolation case is examined, but the focus of the analysis is on real-world measurements. Six major Japanese cities are selected based on population (Tokyo, Osaka, Nagoya and Fukuoka) and geography of Japan, to include the northernmost (Sapporo) and southernmost (Naha) major cities. Some details of these 6 cities are given in Table 1.

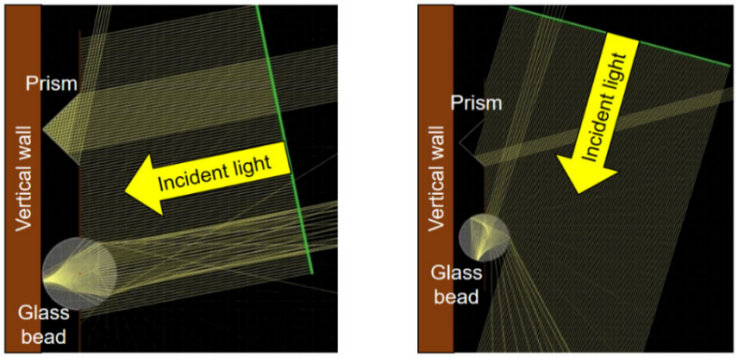

Figure 2. Illustration of how the incident angle of light affects retro reflection of prism-type RRM and bead-type RRM. (L) Small angle (R) Large angle.

Table 1. Information for the 6 Japanese cities examined in this study.

City	Pop. density (ppl./km^2)	Latitude	Longitude	Elevation
Tokyo	1151	35.7°N	139.7°E	25m
Osaka	971	34.7°N	135.5°E	23m
Nagoya	1058	35.2°N	136.9°E	51m
Sapporo	1134	43.1°N	141.3°E	17m
Fukuoka	925	33.6°N	130.4°E	3m
Naha	793	26.2°N	127.7°E	28m

Insolation data and calculation

The insolation data is taken from the New Energy and Industrial Technology Development Organization (NEDO) METPV-20 database sets (NEDO 2023). The data includes direct insolation onto the horizontal (DHI), sunlight hours, global solar radiation, diffuse radiation, temperature, precipitation and more. The records are hourly. For insolation data, the hour represents the sum or average of data for the 60 minutes previous to that hour. The METPV-20 data for direct normal insolation is either measurements or a model based on the Perez diffuse irradiance model (Perez and Seals, 1987), which classifies the sky into 3 parts due to differences in diffusion, one of which is the horizon band (the ring of sky up to 6.5° solar altitude). For the 47 weather stations in Japan with DNI measurement equipment, the measured values are used. For the remaining 788 stations, the DNI values are estimates based on the model. The locations analyzed in this paper are all among the 47 stations with actual DNI measurement data.

The METPV-20 typical years are chosen by ranking months in the years 2010-2018 by their average insolation. Each month closest to the average is chosen to create the typical year. Each month with the highest value is chosen to create the maximum year. Each month with the lowest value is chosen to create the minimum year.

In this research, we evaluate the typical and maximum year data, as well as isolating the hotter period from May-October (6 months) of both typical and maximum years.

Direct Normal Insolation (DNI) measurement in Japan

Since 2005, Japan's AMeDAS(Automated Meteorological Data Acquisition System) stations use rotating mirror type sunshine duration sensors (Eko Instruments MS-093) which periodically reflect direct insolation to a shaded pyroelectric sensor. According to the manufacturer, the error is <10% (Eko 2023). Measured values of DNI over 120W/m^2 are considered direct sunlight in the calculation of hourly sunshine duration (JMA 2023). The mirror revolves every 36 seconds, reflecting direct insolation onto the sensor, yielding a possible 100 positive results in 1 hour. Thus, 50 measurements over 120W/m^2 in 1 hour would be counted as 0.5 hours of direct sunlight.

The newer rotating mirror type sensors (Eko Instruments MS-90) based on the MS-093, measure DNI. The light reflected onto the sensor generates a signal that was found to be proportional to the DNI. According to the manufacturer, the error is <5% when >700W/m^2. According to Po *et al*. (2018) the error can be larger at low solar altitude (under 15°), or DNI values under 700W/m^2, but is still less than 10%.

Sunlight duration and possible east/west bias

Although some symmetry in insolation results can be expected for the east and west facing walls, in that the total insolation in the AM hours and the PM hours should be about the same, causes of bias will include; difference between local solar noon and 12:00 standard time, weather (for example, in the Osaka typical year data 56% of rainfall occurs in the PM), or sky conditions (such as airborne particles).

Tabulating the METPV-20 sunlight duration data by hour for the 6 locations shows there is asymmetry between the AM and PM hours, both for the typical year and maximum year data, as can be seen in Figure 3.

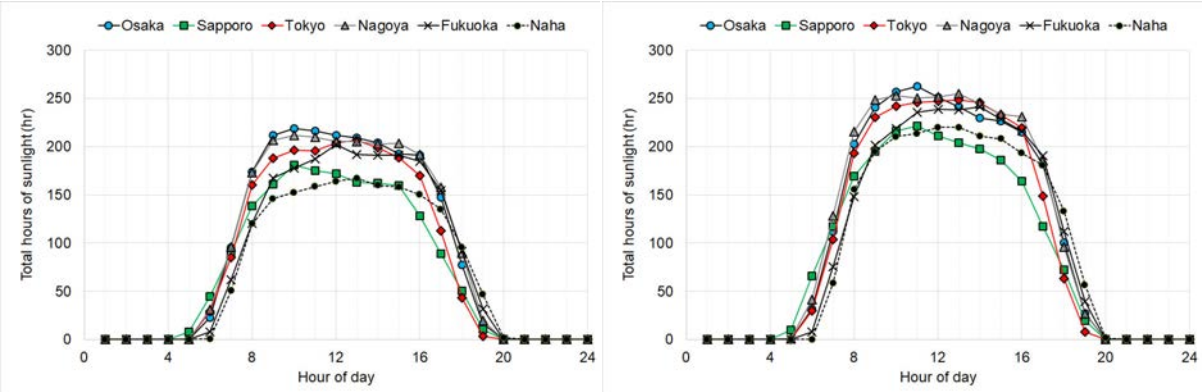

Figure 3. Total annual sunlight hours for 6 major cities in Japan by hour of day. (L) Typical year. (R) Maximum year.

For most cities there is a significant bias for more sunlight in the AM hours, up to 56% in the northern city of Sapporo. Fukuoka and Naha, both in southern Japan and to the west,

show a bias to more sunlight in the PM hours, up to 54% of all sunlight. The total hours are larger for the maximum year, but the ratio of east/west bias is nearly the same. Note that this is not DNI intensity data, but the sunlight hours are based on DNI measurements where any level of DNI over 120W/m^2 is counted equally as sunlight. Thus, a location with a total sunlight hour bias to the west may still have more DI intensity to the east or vice versa.

Calculation of DNI and incident angles for building walls

A program was created in R to calculate the direct insolation (DI) onto building walls over 1 year. The program calculates the solar position for any chosen time, reads in real DHI data from a file corresponding to that time, and uses the trigonometric relations to determine the DI onto walls of chosen angles and tilts. For this study, the solar position calculations are done for 1 year in time steps of 3 minutes, as determined by a sensitivity test of time step length. This time step also allows for resolution of under 1 degree in the compilation of incident angles. The walls are set as facing the 4 compass points, with a tilt angle of 90° (vertical wall). The DHI data read-in is from the hour in which the 3-minute time step occurs. No attempt to create a DHI value by interpolating the hourly data into each time step was made.

For comparison, the theoretical maximum DI values are also calculated for clear skies. Theoretical maximum values of direct insolation are created using the Bouguer equation for the direct insolation I_{DN} above the atmosphere, (ASHRAE 2019) shown in Eq.(1),

$$I_{DN} = 1366\,W/m^2 \times 0.7^{1/\sin h} \quad (1)$$

where 1366W/m^2 is a value for average direct insolation above the atmosphere and h is the solar altitude angle.

Note that this calculation indicates that in theory, the standard value of 120W/m^2 as the minimum cutoff for DNI measurement by the DNI sensors used in Japan will not be met when the sun position is under 8° altitude, thus would not be recorded in the data set. However, as the data set is collated into hourly values, and the sun generally travels 15° across the sky per hour, it is difficult to examine this effect on the real-world data in sufficient detail.

Given this, and the horizon band effect at up to 6.5°, all analysis was done for solar altitude ranging from 6° to 90°. All DNI for solar altitude under 6° was set as zero. A second reason for this step is that unrealistic results are produced at low altitude angles because the DNI data is hourly. For example, if the DNI for 06:00-07:00 is 200W/m^2, and sunrise is at 06:00, the derived value for DI on an east wall at 06:03AM when solar altitude is 0.5° and based on 200W/m^2, is not only theoretically impossible per the Bouguer calculation, but could yield physically impossible DI over 10,000W/m^2 due to the low angle affecting the reverse trigonometric functions.

The calculation of the position of the sun in the sky depends on the equation of time E_t, which is calculated using the algorithm developed by Yamazaki (1980).

The solar azimuth angle, Az and altitude angle, h are calculated by finding the hour angle t in Eq. (2) where T_m is the local decimal time in hours, L is the longitude of the evaluated city, L_o is the longitude of the local standard meridian (for Japan, this is always 135°E). The solar altitude is found with Eq.(3) and the azimuth with Eq.(4), where δ is the solar declination and φ is the latitude of the city. The incident angle i of DI for a given wall of azimuth orientation γ and tilt angle β is then found by Eq.(5). The DHI value is then converted to the DNI with Eq. (6), then into the DI for each wall with Eq. (7).

$$t = 15(T_m - 12) + (L - L_0) + E_t \quad (2)$$

$$\sin h = \cos\varphi \cos\delta \cos t + \sin\varphi \sin\delta \quad (3)$$

$$\sin Az = \frac{\cos\delta \sin t}{\cos h} \tag{4}$$

$$\cos i = \cos h \cos(Az - \gamma) \sin\beta + \sin h \cos\beta \tag{5}$$

$$\mathrm{DNI} = \mathrm{DHI}/\sin h \tag{6}$$

$$\mathrm{DI} = \mathrm{DNI} \cos i \tag{7}$$

Results

The total direct insolation for walls facing the 4 compass points were collated in bins of incidence angle of 10° each. Note that some results may seem counterintuitive at first glance. For example, an early morning sun in winter may have an altitude angle of 7°, but the incident angle to an east facing wall could be over 30° due to the azimuth angle. Similarly, incident angles of DI onto north walls will tend to be large.

Results for Osaka for the typical year, maximum year and theoretical clear sky maximum DI are shown in Figure 4 at left, at right shows the same, restricted to the May-October period of each case. The clear sky values average 55% higher than the real-world maximum year, though trends in which incident angles contribute most to DI are similar. There is some slight east-west asymmetry, with east showing more DI, as expected from the sunlight hour data for Osaka. Over the whole year, angles from 20° to 70° are about equally important on east and west walls while angles 30° to 80° are important for the south wall. DI on the north wall is negligible.

For the May-October period, the results for the south wall are much different, with high angles 70°-80° the greatest contributors. East and west walls are similar to the whole-year values, though a peak shifts to the 20°-30° angle range.

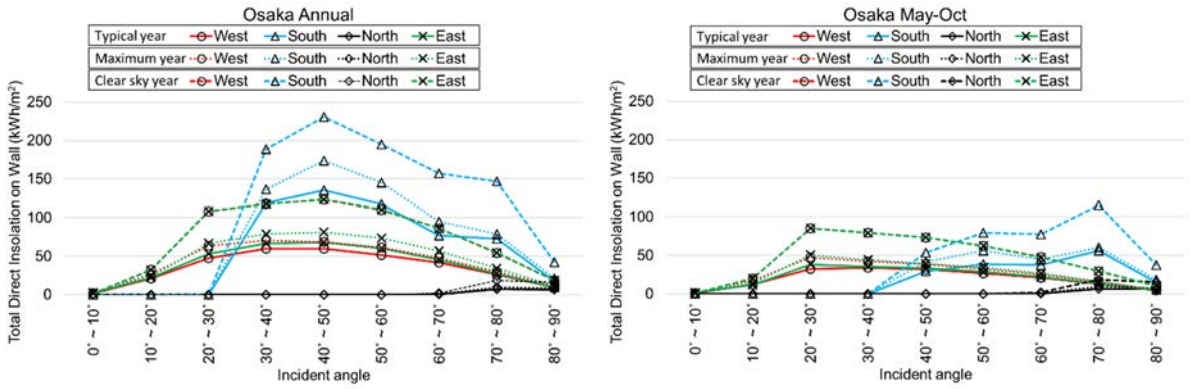

Figure 4. Total annual direct insolation onto 4 walls for Osaka in the typical, maximum, and clear sky years summarized by spans of acceptance angle onto each wall. (L) Whole year data. (R) May-October data.

Results for Sapporo and Tokyo are shown in Figure 5 and Figure 6. Overall, the trends are similar to the Osaka case. There are some local differences. Sapporo has lower DI overall, as expected for a northern city and south-wall DI is not as emphasized compared to east and west walls. Tokyo shows a strong peak for south-facing in the 30°-50° angle range.

All results are presented in a numerical summary in Table 2. Color is added according to the scale as the bottom of the table. Nagoya DI is quite similar to Osaka except for a stronger

dip in the 60°-70° range. Fukuoka and Naha have lower overall DI, despite their southern location. This could be due to more clouds and rain. South-facing walls are the greatest contributors in terms of DI in all cities in typical and maximum years. East and west walls take in about half the DI of a south wall, but combined can exceed the total DI on a south wall. However, in the May-October period, an east or west wall can roughly equal (in Tokyo, Osaka, Nagoya and Fukuoka) or even exceed (in Naha) the total DI on a south wall.

Incident angles of 30°-70° are the greatest contributors for south walls, usually peaking at 40°-50°, except in Tokyo, which peaks at 30°-40°. Incident angles for east and west walls are more uniformly distributed over 20°-70°.

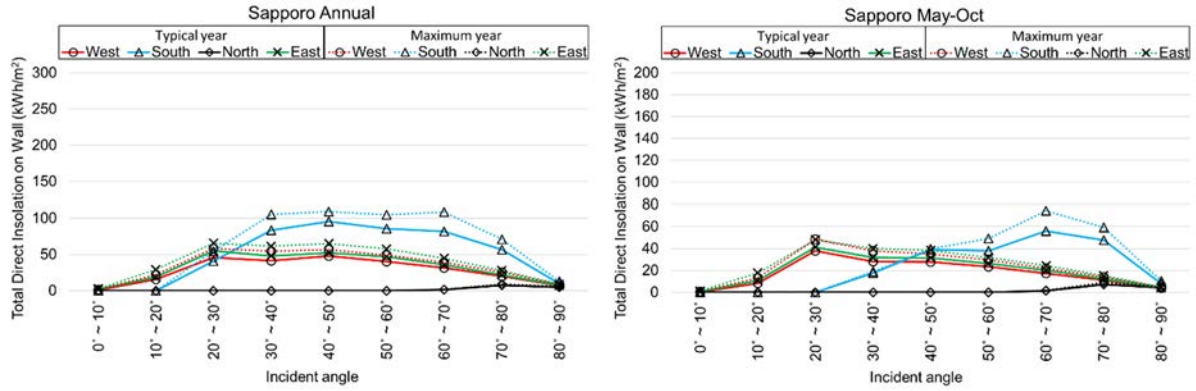

Figure 5. Total direct insolation for Sapporo onto 4 walls in the typical and maximum years. (L) Annual totals. (R) May-Oct totals.

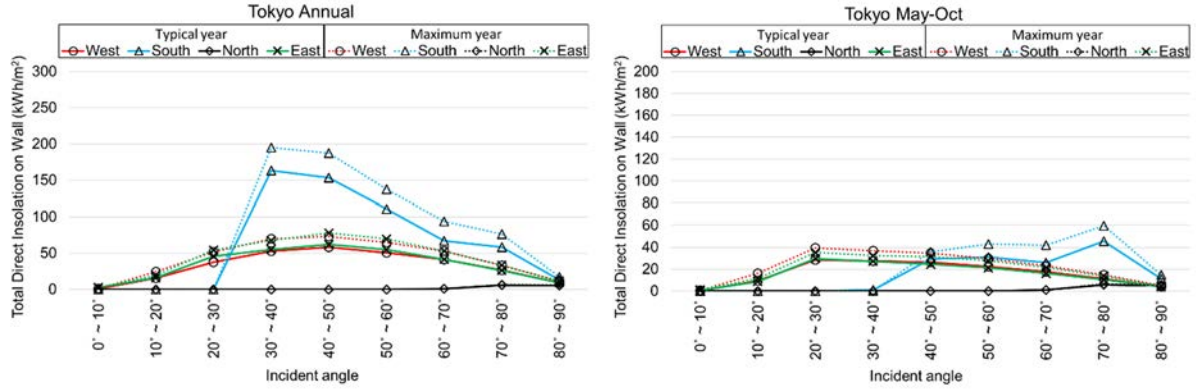

Figure 6. Total direct insolation for Tokyo onto 4 walls in the typical and maximum years. (L) Annual totals. (R) May-Oct totals.

Discussion

The trends in most prevalent incidence angles for each compass direction are generally what could be expected. However, the quantification of the DI and angles using real-world data yields interesting points. For east and west walls, there is a relatively flat distribution of DI intensity over a wide range of angles. Thus, for UHI relief in warm weather, east and west walls may be a better target for RRM application.

For these cities, east walls tend to be exposed to more DI than west walls. Perhaps prioritizing installation of RRM onto east walls could help reduce the morning build-up of heat load in the urban space.

For south-facing walls, angles between 30°-50° are the greatest contributors, but significant DI is still present up to 80°. In the warm period of May-October, the effects at the

south wall can become much more biased to large incident angles. Further, in summer months south walls see no DI for angles below about 40°, due to the location latitude. Sapporo sees some DI in the 30°-40° range, Naha sees no DI under 50°. RRM with high retro reflectance efficiency at incident angles smaller than 40° would be nearly meaningless applied to south walls in most Japanese cities. Application to east and west walls may be able to use common RRM or simpler application that is effective at relatively smaller incident angles. Assuming that common prism/cube-corner RRMs are most effective for incident angles under 45°, they may not be well-suited for use on south-facing walls, and may be almost useless in summer months. They could be somewhat effective on east and west walls. Given the high incident angles for south walls, bead-type RRM may be more suitable. Judgment depends on the retroreflective efficiency of a chosen RRM and costs. Rather than applying RRM sheets directly onto walls, it may be more effective to install RRM material onto angled panels. Awnings or angled siding panels with RRM applied could be much better suited for the most prevalent incident angles. Further analysis on this point is being done. The expected net effect for removing insolation heat load from an urban space, based on RRM efficiency for all angles over the year, is a topic for the next step in this research.

Engineered metamaterials being developed, such as asymmetrical prisms embedded in window films (Yoshida et al. 2014, Kyogoku and Takebayashi 2023) which are designed to reflect incident light upward rather than as perfect retro reflection. The goal of this UHI countermeasure is to remove thermal load from the urban space by upward reflection to the sky at any angle. Perfect retro reflection is less relevant except for the case of upward reflecting onto surrounding tall buildings. Such materials designed to optimally reflect upward sunlight at large incident angles of 70°-80° could be a good solution for south-facing walls in Japan.

With such upward-reflecting materials becoming more common, this analysis can be modified to evaluate the DI over the range of solar profile angles rather than incident angle.

Table 2. Summary of total DI (kWh/m^2) for acceptance angle brackets for all 6 cities, color coded to intensity per the scale at the bottom of the table.

City	Inc. Angle	Annual								May-Oct								City	Annual								May-Oct							
		Typical year				Maximum year				Typical year				Maximum year					Typical year				Maximum year				Typical year				Maximum year			
		S	W	E	N	S	W	E	N	S	W	E	N	S	W	E	N		S	W	E	N	S	W	E	N	S	W	E	N	S	W	E	N
Osaka	0˚ ~ 10˚	0	2	3	0	0	2	2	0	0	1	2	0	0	1	1	0	Naha	0	1	1	0	0	2	2	0	0	1	0	0	0	2	0	0
	10˚ ~ 20˚	0	21	22	0	0	27	24	0	0	12	12	0	0	17	14	0		0	15	20	0	0	21	24	0	0	10	16	0	0	13	17	0
	20˚ ~ 30˚	0	47	53	0	0	64	67	0	0	33	38	0	0	47	51	0		0	49	51	0	0	59	62	0	0	41	40	0	0	46	46	0
	30˚ ~ 40˚	119	60	67	0	136	71	79	0	0	34	36	0	0	42	44	0		0	48	51	0	0	61	67	0	0	33	33	0	0	36	41	0
	40˚ ~ 50˚	136	60	68	0	173	69	81	0	29	32	33	0	42	39	39	0		87	47	47	0	125	61	67	0	1	29	28	0	2	34	39	0
	50˚ ~ 60˚	117	52	61	0	145	61	74	0	39	27	29	0	56	33	35	0		82	41	41	0	111	54	58	0	28	25	23	0	30	31	32	0
	60˚ ~ 70˚	77	42	46	1	95	48	57	1	37	21	22	1	45	25	27	1		59	31	30	3	84	41	43	2	32	18	17	3	41	23	24	2
	70˚ ~ 80˚	73	26	27	7	79	30	35	10	56	13	13	7	60	15	16	10		42	20	21	13	53	26	28	15	26	12	12	13	29	15	15	15
	80˚ ~ 90˚	18	9	9	7	21	11	11	9	15	5	5	6	18	5	5	8		19	7	7	10	26	9	9	12	16	4	4	10	22	5	5	12
	Total	539	319	356	14	651	382	429	20	177	177	189	13	222	225	233	19	Total	289	259	268	26	399	335	361	29	104	172	173	26	125	205	220	29
	Fraction	44%	26%	29%	1%	44%	26%	29%	1%	32%	32%	34%	2%	32%	32%	33%	3%	Fraction	34%	31%	32%	3%	35%	30%	32%	3%	22%	36%	36%	5%	22%	35%	38%	5%
Sapporo	0˚ ~ 10˚	0	1	2	0	0	1	3	0	0	0	1	0	0	1	1	0	Nagoya	0	2	3	0	0	1	3	0	0	1	2	0	0	1	1	0
	10˚ ~ 20˚	0	15	19	0	0	22	29	0	0	8	11	0	0	13	18	0		0	26	19	0	0	29	27	0	0	16	11	0	0	19	15	0
	20˚ ~ 30˚	41	46	55	0	54	58	65	0	0	38	41	0	0	48	48	0		0	58	58	0	0	69	72	0	0	42	42	0	0	52	53	0
	30˚ ~ 40˚	83	42	48	0	105	54	61	0	17	28	32	0	19	38	40	0		139	67	67	0	167	81	83	0	0	33	35	0	1	45	45	0
	40˚ ~ 50˚	95	48	52	0	109	57	65	0	39	28	31	0	40	35	38	0		161	64	70	0	191	77	86	0	30	30	31	0	48	40	41	0
	50˚ ~ 60˚	86	40	47	0	105	49	58	0	38	23	26	0	49	30	32	0		133	56	62	0	157	66	75	0	41	25	27	0	58	33	35	0
	60˚ ~ 70˚	82	31	36	1	109	39	45	2	56	17	20	1	74	22	24	2		82	43	46	1	93	53	56	1	38	19	20	1	42	26	26	1
	70˚ ~ 80˚	57	20	22	7	71	25	28	9	48	11	12	7	59	14	15	9		63	27	28	9	85	33	34	11	46	12	12	9	65	16	16	11
	80˚ ~ 90˚	10	7	7	5	13	8	9	6	8	4	4	4	10	5	5	5		16	9	9	7	21	12	12	9	14	4	4	6	18	6	5	8
	Total	454	249	287	13	566	315	362	16	206	158	178	13	252	205	222	16	Total	595	352	363	17	714	422	448	21	169	181	183	16	232	237	237	20
	Fraction	45%	25%	29%	1%	45%	25%	29%	1%	37%	29%	32%	2%	36%	30%	32%	2%	Fraction	45%	27%	27%	1%	44%	26%	28%	1%	31%	33%	33%	3%	32%	33%	33%	3%
Tokyo	0˚ ~ 10˚	0	1	2	0	0	1	3	0	0	0	1	0	0	1	1	0	Fukuoka	0	1	1	0	0	2	1	0	0	1	1	0	0	1	0	0
	10˚ ~ 20˚	0	16	16	0	0	24	20	0	0	9	9	0	0	16	12	0		0	14	21	0	0	18	25	0	0	9	14	0	0	11	16	0
	20˚ ~ 30˚	0	37	46	0	0	51	54	0	0	28	30	0	0	39	35	0		0	43	46	0	0	58	58	0	0	31	34	0	0	40	43	0
	30˚ ~ 40˚	163	53	55	0	195	70	68	0	1	27	27	0	0	37	32	0		68	49	54	0	89	66	71	0	0	31	32	0	0	39	43	0
	40˚ ~ 50˚	154	58	62	0	187	73	78	0	29	26	24	0	36	35	31	0		110	55	54	0	156	71	71	0	25	31	28	0	38	36	40	0
	50˚ ~ 60˚	111	51	55	0	138	65	70	0	31	22	21	0	43	30	28	0		99	49	47	0	136	63	64	0	38	26	25	0	58	32	35	0
	60˚ ~ 70˚	67	41	42	1	94	53	53	1	26	18	16	1	42	23	22	1		70	37	38	1	96	49	50	1	33	20	20	1	48	26	28	1
	70˚ ~ 80˚	58	27	26	6	76	33	33	7	45	11	10	6	60	15	14	6		63	23	25	7	83	31	31	8	46	12	13	7	61	17	18	8
	80˚ ~ 90˚	13	9	9	5	17	11	11	6	11	4	4	5	15	5	5	5		19	8	8	6	24	11	11	7	17	4	4	6	21	6	6	7
	Total	566	292	313	12	707	381	390	13	144	147	141	11	195	199	180	13	Total	430	278	294	14	583	369	382	17	159	166	172	13	225	208	230	16
	Fraction	48%	25%	26%	1%	47%	26%	26%	1%	32%	33%	32%	3%	33%	34%	31%	2%	Fraction	42%	27%	29%	1%	43%	27%	28%	1%	31%	33%	34%	3%	33%	31%	34%	2%
	Scale	0		20		40		60		80		100		120		140		160	180		200		kWh/m^2										

Conclusions

The analysis here compiled the total DI and its incident angle onto walls in the 4 compass directions for the typical year and maximum year of 6 major cities in Japan. The expectation was that east/west walls would have most DI at lower angles, while the south wall would have much DI at large incident angles, especially during the summer months.

The results showed that south-facing walls are the greatest contributors in terms of DI in all cities examined for both typical and maximum years. East and west walls take in about half the DI of a south wall, but combined can exceed the total DI on a south wall. Incident angles of 30°-70° are the greatest contributors for south walls, usually peaking at 40°-50°, except in Tokyo, which peaks at 30°-40°. For the May-October period, the results for the south wall are much different, with high angles 70°-80° the greatest contributors.

Incident angles for east and west walls are more uniformly distributed over 20°-70°. For May-October, east and west walls are similar to the whole-year values, though the peaks shift to the 20°-30° angle range. In May-October, the total of DI onto the east and west walls will be much larger than onto the south wall. There is some east/west bias in hours of sunlight (time when DI is over 120W/m^2). Osaka, Tokyo, Nagoya and Sapporo have more sunlight in the AM, with Sapporo having the largest bias up to 56%. Fukuoka and Naha, in the southwest of Japan, have more sunlight in the PM, at up to 54%. This trend is true for both annual and warm period (May-October). However, the total amount of DI tends to be greater on the east walls than the west walls in all cities, with a few exceptions at certain angles. RRM application to east walls would tend to be slightly more effective than west walls, due to east/west bias.

North-facing walls have negligible DI, generally under 3% of all DI, except in Naha, where it reaches 5%.

Researchers and manufacturers developing RRM and building applications as a UHI countermeasure in Japan should focus on RRM that are efficient at large incident angles for application to south walls. To remove thermal load from the city during May-October, high efficiency at incident angles smaller than about 40° would be nearly useless in Tokyo, Osaka, Nagoya and Fukuoka, but under 30° in Sapporo and under 50° in Naha.

Application to east and west walls may be an easier target for RRM use, as common RRM materials may be suited for the relatively small incident angles. Further, the total DI on east and west walls far exceeds the south wall in the hotter months.

This analysis method can be supplemented by a focus on solar profile angle rather than incident angle, to help evaluate potential for upward-reflecting metamaterials for UHI relief.

References

Arecchi, A.V., Messadi, T., Koshel,R.J. (2007) *Field Guide to Illumination*, SPIE Press, Bellingham, WA.

ASHRAE (American Society of Heating, Refrigerating and Air-Conditioning Engineers). (2019) *ASHRAE Handbook - HVAC Applications: Solar Energy Use.* ASHRAE. Atlanta.

ASTM International, (2018) *Standard Test Method for Retroreflectance of Horizontal Coatings (ASTM-D4061-13)*

Castellani, B., Morini, E., Anderini, E., Filipponi, M., Rossi, F. (2017). Development and characterization of retro-reflective colored tiles for advanced building skins. *Energy and Buildings*, 154, 513-522. https://doi.org/10.1016/j.enbuild.2017.08.078

Eko Instruments. (2018). *MS-90 DNI Sensor Instruction Manual*. https://www.eko-instruments.com/us/categories/products/dni-sensors/ms-90-dni-sensor [Accessed May, 2023]

Gobakis, K., Kolokotsa, D., Maravelaki-Kalaitzaki, N., Perdikatsis, V., Santamouris, M. (2016). Development and analysis of advanced inorganic coatings for buildings and urban structures. *Energy and Buildings*, 89, 196–205. https://doi.org/10.1016/j.enbuild.2014.10.081

He, B. (2019). Towards the next generation of green building for urban heat island mitigation: Zero UHI impact building. *Sustainable Cities and Society*, 50, 101647. https://doi.org/10.1016/j.scs.2019.101647

Ichinose, M., Inoue, T., Nagahama, T. (2017). Effect of retro-reflecting transparent window on anthropogenic urban heat balance. *Energy and Buildings*, 157, 157-165. https://doi.org/10.1016/j.enbuild.2017.01.051

Inoue, T. (2007). Solar radiation shielding technique. *Building Technology*, 684, 142-145.

JMA (Japan Meteorological Agency) Fukuoka Regional Headquarters. (2023) *Nisshakei no tukumi (The mechanism of pyranometers)* https://www.jma-net.go.jp/fukuoka/kansoku/nissyou.files/nissyou.html [Accessed April 2023]

Levinson, R., Akbari, H. (2010). Potential benefits of cool roofs on commercial buildings: conserving energy, saving money, and reducing emission of greenhouse gases and air pollutants. *Energy Efficiency*, 3, 53-109. doi:10.1007/s12053-008-9038-2

NEDO (New Energy and Industrial Technology Development Organization). (2023) *Nissharyo detabesu etsuran shisutemu (Solar radiation quantity database reference system)* https://appww2.infoc.nedo.go.jp/appww/index.html [Accesssed Jan-May,2023]

Perez, R. & Seals, R. (1987). A new simplified version of Perez diffuse irradiance model for tilted surface. Solar Energy, 39(3), 221 231. https://doi.org/10.1016/S0038-092X(87)80031-2

Pó, M., Hoogendijk, K., Chiba, I., Akiyama, A., Beuttell, W. (2018) Direct Normal Irradiance Measurements Using A Tracker-Less Sunshine Duration Measurement Concept. *35th European Photovoltaic Solar Energy Conference.* Brussels (Belgium), 24-28 September 2018. doi: 10.4229/35thEUPVSEC20182018-6DO.10.5

Rossi, F., Pisello, AL., Nicolini, A., Filipponi, M., Palombo, M. (2014). Analysis of retro-reflective surfaces for urban heat island mitigation: A new analytical model. *Applied Energy*, 114, 621-631. https://doi.org/10.1016/j.apenergy.2013.10.038

Saint-Drenan, Y.M., Wald, L., Ranchin, T., Dubus, L., Troccoli, A. (2018). An approach for the estimation of the aggregated photovoltaic power generated in several European countries from meteorological data. *Adv. in Science and Research*, 15, 51-62. doi:10.5194/asr-15-51-2018.

Santamouris, M. (2014). Cooling the cities–A review of reflective and green roof mitigation technologies to fight heat island and improve comfort in urban environments. *Solar Energy*, 103, 682-703. https://doi.org/10.1016/j.solener.2012.07.003

Tu, Y. (2023). *Open-source Physics Demos & Apps.* https://phydemo.app/ [Accessed May 2023]

Yamasaki, H. (1980). Nissho kankyo no tame no kiso keisanshiki (The Calculation Methods of Solar Environment). *Trans. of Arch. Inst. of Japan*, 288, 139-147. https://doi.org/10.3130/aijsaxx.288.0_139

Yuan, J., Emura, K., Sakai, H., Farnham C., Lu, S., (2016). Optical analysis of glass bead retro-reflective materials for urban heat island mitigation, *Solar Energy*, 132, 203-213. https://doi.org/10.1016/j.solener.2016.03.011.

Yuan, J., Farnham C., Emura, K. (2015). Development of a retro-reflective material as building coating and evaluation on albedo of urban canyons and building heat loads, *Energy and Buildings*, 103, 107-117. https://doi.org/10.1016/j.enbuild.2015.06.055.